Lateral Instabilities in a Grafted Layer in a Poor Solvent

Chuck Yeung,[†,‡,§] Anna C. Balazs,[*,†] and David Jasnow[‡]

Materials Science and Engineering, University of Pittsburgh, Pittsburgh, Pennsylvania 15261, and Department of Physics and Astronomy, University of Pittsburgh, Pittsburgh, Pennsylvania 15260

Received October 13, 1992; Revised Manuscript Received January 5, 1993

ABSTRACT: The effect of solvent quality on a layer of end-grafted polymers is determined using the random phase approximation combined with a numerical mean field analysis. For sufficiently poor solvents, the laterally homogeneous grafted layer is linearly unstable to fluctuations tangential to the grafting plane. In the unstable regime, the grafted layer forms a "dimpled" surface in which the depth and separation of the dimples depend on chain length, solvent quality, and grafting density.

I. Introduction

The presence of polymers can dramatically influence the properties of both penetrable and impenetrable interfaces and can in turn modify bulk phase behavior.[1,2] For exmple, diblock copolymers can be used as emulsifying agents in otherwise incompatible blends, and polymers grafted to surfaces of colloidal particles can prevent flocculation. However, the ability to theoretically predict the interfacial behavior in these spatially inhomogeneous polymer systems remains an outstanding challenge. At high polymer concentrations, mean field methods can be used to obtain the polymer concentration profile.[3-11] The random phase approximation (RPA)[3,12] can then be used to analyze the stability of the mean field solution.[13] To date, application of the random phase approximation for heterogeneous systems has been limited to cases in which the mean field profile is either known analytically or may be otherwise assumed.[14-16] However, the mean field analysis can, in general, be performed numerically,[4-8] which can greatly expand the domain for RPA applications. In this paper, we combine the random phase approximation with a numerical mean field analysis to study the effect of solvent quality on a layer of homopolymers in which one end of the polymers is grafted to a planar, impenetrable surface. We consider the case in which the grafting points are fixed; i.e., the grafted ends cannot move on the surface.

In the strong stretching limit, the mean field theory for end-grafted polymers in a good solvent can be solved analytically using the classical path approximation.[10,11] Applying the random phase approximation, Marko and Witten studied the linear stability of the mean field solution for a blend of grafted A-type and B-type chains.[14] It was found that the grafted layer can undergo a rippling transition as the A-B incompatibility is increased. That is, due to the fixed grafting points, global phase separation is impossible but, as indicated by the fact that the instability of the mean field solution occurs at finite wavelength, a microphase separation occurs tangential to the grafting plane. However, for an end-grafted *homopolymer* layer in a *poor solvent* the situation is more complicated. The effect of decreasing the solvent quality will be to increase the local monomer concentration. This can occur in two ways: First there may be local clumping of the polymer chains in the tangential direction, leading to a rippling transition similar to that of the A-B mixture. However, decreasing the solvent quality will also cause the entire end-grafted layer to compress normal to the grafting plane. This effect will make the layer more stable against tangential fluctuations, and the rippling transition may be suppressed. The Monte Carlo simulations of Lai and Binder[19] and the molecular dynamics simulations of Grest and Murat[20] show that, at least for some regimes, the lateral phase separation occurs. A scaling argument by Klushin also indicates that such a transition may occur.[21] On the other hand, an RPA analysis by Ross and Pincus which assumes that the polymer concentration profile is a step function indicates that such a transition does not occur,[15] so the question remains unresolved.

To probe the apparent contradictions further, we study the end-grafted layer by combining the random phase approximation with a numerical mean field analysis. We find that, for fixed chain length and grafting density, the grafted layer is unstable to tangential fluctuations in a sufficiently poor solvent. We construct the phase diagram as a function of chain length, grafting density, and solvent quality, separating the regimes in which the laterally homogeneous layer is linearly stable from that in which it is linearly unstable. When the mean field solution becomes unstable, our analysis indicates that, tangential to the grafting plane, the end-grafted polymers clump together to form a "dimpled" surface. For shorter chains, the depth of the dimples approximately equals the layer height, and the mean distance between dimples is proportional to the radius of gyration of the chain in a Θ-solvent. As the chain length is increased, the instability is more and more restricted to a region near the edge of the grafted layer. A dimpled structure is still formed, but the depth of the dimples is now given by the bulk correlation length. The mean distance between the dimples is larger than the radius of gyration.

The instability of the layer does not result if a step function is used for the mean field profile on which RPA fluctuations are built.[15] The classical path approximation can also be applied to the poor solvent situation.[17,18] We argue below that a stability analysis of the concentration profile obtained from the classical path approximation also will not produce the instability of the grafted layer. (This is true even though our stability analysis is the same as that of Marko and Witten.[14]) In order to obtain the instability, it appears that the correct mean field solution must be obtained, and at least for the present, the mean field solution must be obtained numerically. Since the mean field solution and its stability in the present case depend on the solvent quality, we find the rich behavior outlined above. Since it does not require an analytic mean

* Author to whom correspondence should be addressed.
† Materials Science and Engineering.
‡ Department of Physics and Astronomy.
§ Present address: Department of Physics, University of Toronto, Toronto, ON, Canada M4S 1A7. E-mail: yeung@vishnu.physics.utoronto.ca.

0024-9297/93/2226-1914$04.00/0 © 1993 American Chemical Society

field solution, our approach is quite general and should allow one to study the effect of fluctuations in a large class of spatially inhomogeneous polymer systems.

II. Mean Field Analysis

We describe the end-grafted polymers with the Edwards Hamiltonian,[3]

$$\mathcal{H}\{\mathbf{R}_b(m)\} = \frac{1}{2a^2}\sum_b \int_0^N dm \left|\frac{\partial \mathbf{R}_b(m)}{\partial m}\right|^2 + \int d\mathbf{r}\left(\frac{w_2 a^3}{2}c(\mathbf{r})^2 + \frac{w_3 a^6}{3}c(\mathbf{r})^3\right) \quad (2.1)$$

where a is the bond length, N is the polymerization, $\mathbf{R}_b(m)$ is the position of the mth monomer on the bth chain, and $c(\mathbf{r})$ is the local monomer concentration at a point $\mathbf{r}$. We denote a vector in the x–y plane by $\mathbf{x}$ and the coordinate normal to the grafting plane by z, i.e., $\mathbf{r} = (\mathbf{x},z)$. The grafting point of the bth chain, $\mathbf{R}_b(0)$ is fixed on the grafting plane $z = 0$ and $c(\mathbf{r}) = 0$ for $z < 0$. The grafting density is $1/l^2$, where l is the average distance between grafts. We have absorbed the factor of k_BT in $\mathcal{H}$ so that the Hamiltonian is dimensionless. The first term in the Hamiltonian is due to the connectivity of the chain. The second term comes from the solvent-mediated two-body interaction, and $w_2 > 0$ (<0) for a good (poor) solvent.[22a] The third term is due to three-body interactions, and $w_3 > 0$. In a good solvent w_3 is irrelevant after renormalization and can be neglected. However, for a poor solvent this term must be included.[22b]

The local monomer concentration is given by

$$c(\mathbf{r}) = \sum_b \int_0^N dm\, \delta(\mathbf{R}_b(m) - \mathbf{r}) = \langle c(\mathbf{r})\rangle + \delta c(\mathbf{r}) \quad (2.2)$$

where the brackets indicate the thermal average and $\delta c(\mathbf{r})$ is the deviation of the local concentration from the average so $\langle \delta c(\mathbf{r})\rangle = 0$. Substituting eq 2.2 into eq 2.1, the mean field Hamiltonian $\mathcal{H}_0$ can be obtained from $\mathcal{H}$ by neglecting all terms of order δc^2 or higher,[4]

$$\mathcal{H}_0\{\mathbf{R}_b(m)\} = \frac{1}{2a^2}\sum_b \int_0^N dm \left|\frac{\partial \mathbf{R}_b(m)}{\partial m}\right|^2 + w_2 a^3\langle c(\mathbf{R}_b(m))\rangle + w_3 a^6 \langle c(\mathbf{R}_b(m))\rangle^2 \quad (2.3)$$

and

$$\int dz\, \langle c(z)\rangle = N/l^2 \quad (2.4)$$

where $\langle c(z)\rangle$ is the value of $\langle c(\mathbf{r})\rangle$ averaged over the tangential (x–y) plane. Within the mean field approximation, the interacting polymer system is reduced to a system of independent chains in the self-consistent field of the other chains. We assume that the mean field solution is laterally homogeneous, i.e., $\langle c(\mathbf{r})\rangle = \langle c(z)\rangle$, and perform a linear stability analysis of the mean field concentration profile.

By rescaling z, $\mathbf{x}$, m, and c, it can be shown that there are only two dimensionless parameters. The rescalings appropriate for a poor solvent are[18]

$$\tilde{z} = z/h, \quad \tilde{x} = x/X_0, \quad s = m/N, \quad \tilde{c}(\mathbf{r}) = c(\mathbf{r})/c_0 \quad (2.5)$$

where $X_0 = (a^2N/2)^{1/2}$ is the radius of gyration of the chain in a Θ-solvent, $h = Nw_3a^3/(|w_2|l^2)$ is the characteristic layer height in the strong stretching limit, and $c_0 = |w_2|/(w_3a^3)$ is the bulk equilibrium concentration. With this rescaling, the two dimensionless parameters are $\gamma = h^2/(2X_0^2) = N(w_3^2a^4)/(|w_2|^2l^4)$ and $\beta = (|w_2|^4l^4)/(w_3^3a^4)$.[18] Physically, γ is a parameter describing the stretching of the chains in the z direction relative to the chains' lateral extension. The parameter β is less easily interpreted but can be thought of as a measure of the interaction vs connectivity terms in the Hamiltonian. The strong stretching limit (in which the classical path approximation holds) is obtained by letting $\gamma \to \infty$.[18] A detailed derivation of this rescaling along with its relevance to the strong stretching limit is given in Appendix A.

III. Numerical Random Phase Approximation

Although systems in which the mean field analysis can be performed analytically are rare,[9-11] extensive numerical techniques have been developed.[4-8] In most cases only single-point quantities are considered, but since the chains are independent, the two-point correlation function of the mean field Hamiltonian

$$A^0(\mathbf{r},\mathbf{r}') \equiv \langle c(\mathbf{r})\, c(\mathbf{r}')\rangle^0 - \langle c(\mathbf{r})\rangle^0 \langle c(\mathbf{r}')\rangle^0 \quad (3.1)$$

can also be calculated numerically. (Here the superscript "0" indicates the averages are with respect to $\mathcal{H}_0$, the independent chain Hamiltonian.) The random phase approximation is essentially an expansion of the full Hamiltonian $\mathcal{H}$ in terms of the concentration fluctuations around the mean field solution. At lowest order, the RPA relates the correlation function A of the full Hamiltonian (i.e., including interchain correlations) to A^0,

$$[A]^{-1}(\mathbf{r},\mathbf{r}') = [A^0]^{-1}(\mathbf{r},\mathbf{r}') + (w_2a^3 + 2w_3a^6\langle c(\mathbf{r}')\rangle^0)\,\delta(\mathbf{r} - \mathbf{r}') \quad (3.2)$$

where the nonsuperscripted quantities are the RPA expectation values.

The correlation function A is proportional to the response of the local monomer concentration to an external perturbation. Therefore, in addition to describing equilibrium fluctuations, the correlation function contains information about the stability of the mean field solution. In particular, if any of the eigenvalues ϵ_i of A^{-1} are *negative*, the mean field solution is linearly unstable. (For this reason A^{-1} is also known as the stability matrix.) The corresponding eigenvector ϕ_i with the most negative eigenvalue ϵ_i is the most unstable mode. Although a full description of the structures that are formed in the unstable regime would generally require an analysis of higher order (in δc) corrections to $\mathcal{H}_0$, the mode ϕ_i which becomes unstable as the phase boundary between stable and unstable regimes is crossed often describes the structures that are formed.[23] Therefore, the linear stability analysis can be used to determine both the stability of the laterally homogeneous grafting layer and, hopefully, the type of structures formed as the phase boundary is crossed.

Several cautionary remarks are in order. The linear analysis cannot rule out the possibility that the laterally homogeneous state is metastable and that a first-order phase transition changes the layer structure before the linear instability sets in. In this paper, we will assume that this is not the case. Deeper into the unstable region, it is much less likely that the structures observed will be given by the most unstable linear mode. Therefore, we restrict the discussion to the structures formed as the phase boundary between the linearly stable and unstable regimes is crossed.

To solve the mean field problem we use the Green's function formalism.[3] The independent chain Green's function factors as

$$G(\mathbf{r},m;\mathbf{r}',m') = G_0(\mathbf{x},m;\mathbf{x}',m)\, F(z,m;z',m') \quad (3.3)$$

where G_0 is the Green's function in the x–y plane and is

given by the diffusion propagator

$$G_0(\mathbf{x},m;\mathbf{x}',m) = 0 \quad \text{for } m < m'$$

$$= (2\pi a^2|m-m'|)^{-1} \exp\left(-\frac{|\mathbf{x}-\mathbf{x}'|^2}{2a^2|m-m'|}\right) \quad \text{for } m \geq m' \quad (3.4)$$

The function F satisfies[3]

$$\left(\frac{\partial}{\partial m} - \frac{a^2}{2}\frac{\partial^2}{\partial z^2} - w_2 a^3\langle c(z)\rangle - w_3 a^6\langle c(z)\rangle^2\right)F(z,m;z',m') = \delta(z-z')\,\delta(m-m') \quad (3.5)$$

Both the average concentration $\langle c(z)\rangle$ and the mean field correlation matrix A^0 can be obtained from the Green's function. The explicit formulas for $\langle c(z)\rangle$ and A^0 in terms of the Green's functions are given in Appendix B.

The mean field concentration is obtained by a standard iterative process. The Green's function is evaluated by numerically solving eq 3.5 using a trial concentration $\langle c(z)\rangle$. A new trial concentration is obtained from the Green's function, and the process is repeated until convergence is reached. Here convergence is operationally defined by the criterion

$$\frac{\int dz\,|\langle c'(z)\rangle - \langle c(z)\rangle|}{\int dz\,\langle c(z)\rangle} < 10^{-7}$$

where $c(z)$ is obtained from the Green's function using $c'(z)$ as the trial function in eq 3.5. After convergence we calculate the mean field correlation function given by eq B8 in Appendix B. Due to the translational invariance in the x–y plane, the eigenvectors of A^0 (and of A) are of the form $\phi_{i,q}(z)\exp(-i\mathbf{q}\cdot\mathbf{x})$, and

$$\int d\mathbf{x}\int d\mathbf{x}'\,A^0(\mathbf{r},\mathbf{r}')e^{i(\mathbf{q}\cdot\mathbf{x}+\mathbf{q}'\cdot\mathbf{x}')} = \delta(\mathbf{q}+\mathbf{q}')\,A^0(z,z';q) \quad (3.6)$$

where $\mathbf{r} = (\mathbf{x},z)$ and $\mathbf{q}$ is the wavenumber in the x–y plane.

In practice, we integrate eq 3.5 using an Euler discretization with $\Delta m = {}^1/_8$ and $\Delta z = {}^1/_2$. We discretize A^0 using the same value of Δz and perform the Fourier transform with respect to $\mathbf{x}$ explicitly. For each value of q, the result is a square matrix $A^0(z,z';q)$ which we invert to calculate $A^{-1}(z,z';q)$ using eq 3.2. We then obtain the eigenvalues $\epsilon_i(q)$ and eigenvectors $\phi_i(q)$ of $[A]^{-1}$.[25]

For numerical reasons, it is simpler to fix N and vary w_2 and w_3. Our mean field analysis is done with $N = 64$, $l^2 = 5$, and $a = 1$. Since the stability depends on only the two dimensionless parameters $\gamma = N(w_3{}^2a^4)/(|w_2|^2l^4)$ and $\beta = (|w_2|^4l^4)/(w_3{}^3a^4)$, we can rescale our results to any other values of N, l^2, and a.

To study the stability of the grafted layer in a poor solvent, we fix w_3 and vary w_2 until we can identify, to within 0.2%, the value of w_2 at which the lowest eigenvalue of A^{-1} vanishes. In this manner, we obtain numerically the critical value, $\beta = \beta^*(\gamma)$, at which the mean field solution becomes linearly unstable. The process also yields the critical wavenumber $q^*(\gamma)$ of the first unstable mode which gives the characteristic lateral length scale of the structures formed as the phase boundary is crossed. The critical eigenvector $\phi^*(z;\gamma)$ gives the z dependence of the structures formed at the phase boundary.

IV. Results

We first present the results of the linear stability analysis. Figure 1 shows the phase boundary separating the regime in which the mean field concentration profile is stable from that in which it is unstable. (Linear stability and instability are implied unless otherwise stated.) For any finite γ, the laterally homogeneous profile is stable for sufficiently small β and unstable for sufficiently large β. The phase boundary can be divided into small- and large-γ regimes. At small γ, the critical value of β is observed to behave as $\beta^*(\gamma) \sim \gamma^{-3/2}$. We will present an argument for this in the next section. There is a crossover between $\gamma \approx 0.1$ and $\gamma \approx 0.5$. At large γ we find that the phase boundary is given empirically by $\beta^*(\gamma) \sim \gamma^{-\alpha}$, where $\alpha \approx {}^3/_4$.

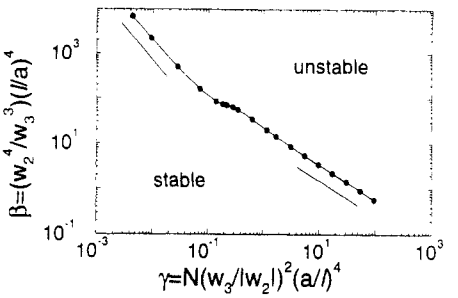

Figure 1. Stability diagram as a function of γ and β. The circles are the values of γ at which $\beta^*(\gamma)$ is determined. The mean field solution is linearly stable for $\beta < \beta^*$ and unstable for $\beta > \beta^*$. The line at large γ has a slope of $-{}^3/_4$. The line at small γ has a slope $-{}^3/_2$.

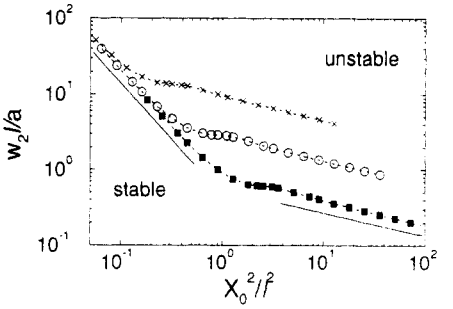

Figure 2. Stability diagram as a function of the experimental control parameters $X_0{}^2/l^2$ and w_2a/l. Three values of w_3 are shown: (×) $w_3 = 8$; (○) $w_3 = 1$; (■) $w_3 = {}^1/_8$. The slope of the solid line on the left is $-{}^3/_2$ while that of the line on the right is $-{}^3/_{10}$. Note that the phase boundaries for the different values of w_3 collapse in the small-γ regime.

In a typical experiment, w_3 and the grafting density will be fixed and w_2 and N will be varied. In Figure 2, we plot the phase boundary in terms of the ratio of $X_0{}^2/l^2 = \gamma(\beta/(4w_3))^{1/2}$ vs $w_2(l/a) = \beta^{1/4}w_3{}^{3/4}$ for various values of $w_3 = 8$, 1, and ${}^1/_8$. (w_3 is expected to be of order unity, and X_0 is the radius of gyration of the chain in a Θ-solvent.) The phase boundaries in the two regimes are described by the empirical scaling relations $w_2(l/a) \sim (X_0/l)^{-3}$ in the small-γ regime and $w_2(l/a) \sim (X_0/l)^{-3/5}$ in the large-γ regime. Note that the phase diagram shows that for fixed solvent quality (w_2 and w_3) and grafting density (l^{-2}) the laterally homogeneous concentration profile is unstable with increasing chain length N ($\sim X_0{}^2$). We will discuss the scaling relations and the observability of the two regimes in the next section.

Figure 3 shows the scaled critical lateral wavenumber, $q^*(\gamma)X_0$, at which the instability occurs. Due to the fixed grafting points, the polymers cannot slide on the grafting plane, and the instability cannot occur at $q = 0$. Similar to Figure 1, there are two distinct regimes in Figure 3. For small γ, we find $q^*X_0 \approx 1.375$ independent of γ and so in the lateral direction, the instability length scale is $2\pi/q^* \approx 4.5X_0$. A crossover in q^*X_0 occurs at the same values of γ as for the phase boundary. In the crossover region q^*X_0 becomes γ dependent and so for large-γ, we observe

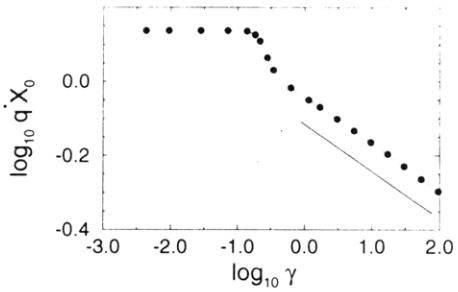

Figure 3. Critical wavenumber $q^*(\gamma)$ at which the instability occurs as a function of γ. For small γ, $q^*(\gamma)$ is at the same value as that of the independent chain system. At larger γ, the most unstable mode occurs at larger length scales. Empirically we find that $q^*X_0 \sim \gamma^{-1/8}$ (solid line) at large γ.

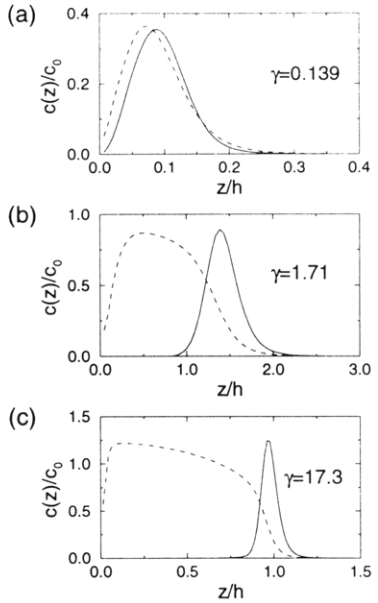

Figure 4. Critical eigenvector $\phi^*(z;\gamma)$ (solid line) along with the scaled concentration (dashed line) at the phase boundary. $c(z)$ is scaled by $c_0 = |w_2|/(w_3a^3)$ and z by $h = Nw_3a^3/(|w_2|l^2)$. Three values of γ are shown: (a) $\gamma = 0.139$, (b) $\gamma = 1.71$, and (c) $\gamma = 17.3$.

that $q^*X_0 \sim \gamma^{-b}$ with $b \approx 1/8$ (as indicated by the solid line in Figure 3). Therefore q^*X_0 decreases with increasing γ and so instability occurs at larger length scales. This indicates that the chains are becoming stretched in the tangential direction.

Figure 4 shows $\phi^*(z;\gamma)$, the z dependence of the critical eigenvector together with the scaled concentration profiles at the phase boundary between the stable and unstable regimes. The figures show the rescaled variables $c/c_0 = cw_3a^3/|w_2|$ and $z/h = z/(Nw_3a^3)/(|w_2|l^2)$. Figure 4a, with $\gamma = 0.139$, corresponds to the small-γ regime. The critical eigenvector occupies most of the grafted layer and, therefore, the instability involves the entire layer. As γ is increased to $\gamma = 1.71$ (Figure 4b) and finally to $\gamma = 17.3$ (Figure 4c), the most unstable mode is increasingly restricted to the edge of the grafted layer, and the fraction of the layer occupied by the instability is a decreasing function of γ.

V. Discussion

In this section we discuss qualitatively the reasons for the different features of the instability for small and large γ. To help clarify the dimensionless parameters, we can consider the system to be close to the Θ-temperature with w_2 small and negative and w_3 fixed. One can then imagine increasing γ by increasing the grafting density l^{-2}. In the small-γ regime, at the instability, the concentration is relatively dilute, less than the bulk equilibrium value c_0. In this case the w_3 term in the Hamiltonian can be neglected. Increasing the grafting density will increase γ, and the monomer concentration will become comparable to c_0. This corresponds to the large-γ regime, where the w_3 terms are important.

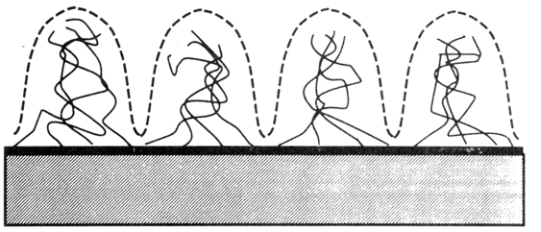

Figure 5. Schematic showing the types of structures expected in the small-γ region. The instability occurs over the entire layer, which is in this case on the order of X_0, and the most unstable wavenumber is at $q = 1.375/X_0$. This implies a dimpled structure with the depth of the dimples being the layer height and lateral distance between dimples of about $4X_0$.

A. Small-γ Regime. In the small-γ regime, $q^*X_0 \simeq 1.375$ independent of γ, indicating that the lateral instability occurs on the order of the Θ-solvent radius of gyration X_0. In the normal direction, the instability occurs over almost the entire layer (see Figure 4a). We conclude that the end-grafted layer forms a dimpled surface with the distance between dimples on the order of the radius of gyration, X_0, and the depth of the dimples being on the order of the layer height (shown schematically in Figure 5).

In this regime, the mean field concentration profile is essentially that of the Gaussian end-grafted chains in zero potential ($w_2 = w_3 = 0$). For example, the difference between $\langle c(z)\rangle$ for $\gamma = 0.139$ and $\langle c(z)\rangle$ for $w_2 = 0$, $w_3 = 0$ is less than 2% over the entire layer. (As noted previously, the discussion is restricted to values of β along the phase boundary.) This means that the solvent effects come into the stability analysis only through the RPA corrections (the last two terms on the right-hand side of eq 3.2) and not in the modification of the independent chain correlation A^0. Since $\langle c(z)\rangle$ is the same as that for $w_2 = w_3 = 0$ and the dimpling occurs, the compression of the layer can be neglected relative to the clumping of the polymers in the tangential plane.

We can, in the expression for A^{-1} (eq 3.2), replace A^0 by the correlation function for the end-grafted Gaussian chain in zero potential ($w_2 = w_3 = 0$). Furthermore, from Figure 2, the curves for different values of w_3 collapse in the small-γ regime, so that the w_3 term is unimportant in the stability analysis. In that case, the RPA correction, $w_2\delta(\mathbf{r} - \mathbf{r}')$, is just proportional to the identity matrix. The eigenvectors of A^{-1} are the same as those of $[A^0]^{-1}$, and the eigenvalues of A^{-1} are simply related to the eigenvalues of $[A^0]^{-1}$ by the shift $\epsilon_i(q) = \epsilon_i^0(q) + w_2a^3$. The result is that in the small-γ regime the most unstable mode of A is always the most unstable mode of A^0. We conclude that q^*X_0 and the shape of $\phi^*(z,\gamma)$ should be independent of γ.

Using A^0 for an end-grafted layer in a Θ-solvent, we find the minimal eigenvalue for $[A^0]^{-1}$ occurs at $q = q^* = 1.375/X_0$ and has the value $0.636l^2a^4X_0^{-3}$. Substituting this into eq 3.2 and neglecting the w_3 term, the laterally homogeneous solution becomes unstable at

$$w_2 = -1.80\left(\frac{l}{a}\right)^2\left(\frac{1}{N}\right)^{3/2} \tag{5.1}$$

in agreement with our numerical results.

The behavior in the normal direction can be understood as follows. Returning to eq 3.2, the RPA correction in A^{-1} is stabilizing if $\langle c(z)\rangle > c_0/2$, where $c_0 = |w_2|/(w_3a^3)$, and destabilizing for $\langle c(z)\rangle < c_0/2$. In the small-$\gamma$ regime, $\langle c(z)\rangle$ is less than $c_0/2$ in the entire layer (see Figure 4a). Therefore, the width of the unstable mode is over the entire layer. For a Θ-solvent, the layer height is of order X_0.

The behavior of the phase boundary for small γ can also be obtained from a scaling argument. Let H be the height of the end-grafted layer. The elastic energy per chain is on the order of H^2/X_0^2 for $H > X_0$ and X_0^2/H^2 for $H < X_0$.[26] Since, for a Θ-solvent, H is of order X_0, the elastic energy per chain is of order unity. Since the w_3 term is unimportant in the stability analysis, the volume interaction energy per chain is of order w_2a^3Nc, where $c \sim N/(l^2H)$. The instability will occur when the interaction energy is the same magnitude as the elastic energy, or, since $H \sim aN^{1/2}$,

$$-w_2a^3Nc \sim -\frac{w_2N^{3/2}a^2}{l^2} \sim 1 \tag{5.2}$$

or $-w_2 \sim (l/a)^2N^{-3/2}$, in agreement with eq 5.1. We note that this scaling argument gives a different result from that of Klushin,[21] who assumed that the concentration is given by the bulk equilibrium value.

B. The Crossover. In the small-γ regime, as discussed above, $\langle c(z)\rangle$ is not greatly affected by the solvent quality. The crossover occurs when the effects of the poor solvent, the compression of the entire polymer layer, and the lateral clumping of the layer become comparable. This occurs when the three-body interactions become important. Since in the small-γ regime the elastic energy and two-body interaction energy are comparable (along the phase boundary), we can estimate where the small-γ regime ends by matching the elastic, the two-body, and the three-body interactions. The latter two match when $c \sim c_0$. Then using $c \sim N/(l^2H)$ we have

$$\left(\frac{H}{X_0}\right)^2 \sim -w_2a^3\frac{N^2}{l^2H} \sim w_3a^6\frac{N^3}{l^4H^2} \tag{5.3}$$

Substituting the small-γ result, $H \approx X_0$, we find that the crossover of the phase boundary occurs when

$$-w_2 \sim \left(\frac{l}{a}\right)^2\frac{1}{N^{3/2}} \sim w_3\left(\frac{a}{l}\right)^2N^{1/2} \tag{5.4}$$

where the first line comes from matching the first pair of terms and the second line comes from matching the second pair. This yields the crossover at $w_3 \approx (l/a)^4N^{-2} \approx l^4/X_0^4$. For $X_0^4/l^4 \leq w_3^{-1}$, we are in the small-γ regime. However, if X_0^2/l^2 is too small, our analysis breaks down. Since w_3 is expected to be of order unity, the small-γ regime as produced by our analysis may be difficult to observe. Note, however, that the Monte Carlo results of Lai and Binder[19] show that even for l^2 somewhat larger than X_0^2 the polymers do not form individual isolated globules but rather clump together in larger groupings. Therefore, our analysis in terms of cooperative behavior of chains may be helpful in understanding the behavior of the end-grafted layer even for l^2 greater than X_0^2.

Another feature of the crossover regime is that the instability no longer occurs over the entire layer but is increasingly restricted to the edge of the layer (see Figure 4b). We can understand this by simply noting that there are some z such that $\langle c(z)\rangle > c_0/2$. Therefore the RPA correction is stabilizing in this inner region. The instability is therefore restricted to the top of the grafted layer where $\langle c(z)\rangle < c_0/2$ but $\langle c(z)\rangle$ is nonnegligible.

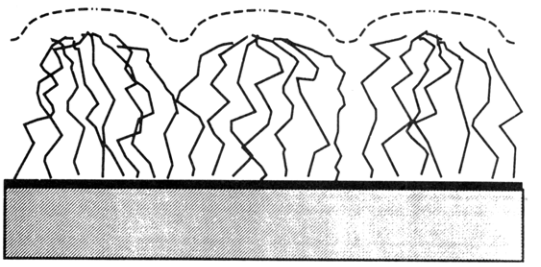

Figure 6. Schematic showing the types of structures expected in the large-γ region. A dimpled surface is again formed. However, the instability is restricted to a region near the top of the grafted layer on the order of the bulk correlation length, and the distance between the dimples is larger than the Θ-solvent radius of gyration X_0.

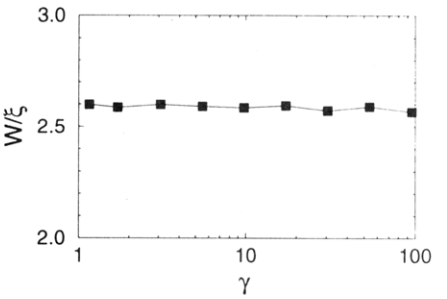

Figure 7. Width of the unstable mode, W, divided by the bulk correlation length $\xi = aw_3^{1/2}/w_2$ vs γ for larger values of γ. This shows that, in the normal direction, the instability occurs on length scales on the order of the bulk correlation length.

C. Large-γ Regime. In the large-γ region, most of the grafted layer has $\langle c(z)\rangle > c_0/2$. In this region, the RPA correction is stabilizing and the instability is restricted to the top of the grafted layer. Figure 6 shows schematically the types of structures we expect from the linear stability analysis in the large-γ region.

Since the instability is restricted to the region in which $\langle c(z)\rangle$ changes from $c_0/2$ to zero, it should be on the order of the width of the interface between bulk chains and solvent. This, in turn, is on the order of the bulk correlation length. For a poor solvent the bulk correlation length is $\xi = (ac_0|w_2|)^{-1/2}$ or $\xi = aw_3^{1/2}/|w_2|$. Figure 7 shows the constant value of the width of the unstable mode divided by the bulk correlation length. Here, the width of the unstable mode is taken to be at half-maximum. Note that the large-γ regime, which does indeed yield a more steplike profile at the instability, does not imply a very poor solvent ($|w_2| \gg 1$) in which the correlation length would be on monomeric length scales. The large-γ instability can be approached by maintaining the system very close to the Θ-temperature and increasing the chain length or grafting density. Under such conditions the correlation length is much larger than monomeric length scales.

Figure 3 shows that q^*X_0 is a decreasing function of γ. Therefore in the lateral direction, the instability occurs on length scales larger than X_0. We conjecture that this feature is due to the following. As γ becomes larger, the instability becomes restricted to the tips of the chains. Since the tips of the chains will have the greatest freedom to move in the lateral direction, the distance between the dimples increases as a function of γ.

Finally, we note that at the top of the layer, the mean field theory is least accurate. Therefore in the large-γ regime, detailed results of this analysis, such as exponent values, may not be accurate. However, we expect that

qualitative results, such as the existence of the instability and the length scale over which this instability occurs, will still be valid.

D. Classical Path Approximation in the Case of a Poor Solvent. For a good solvent, the classical path approximation has proven to be a very useful method.[10,11] (This approximation neglects all fluctuations around the path minimizing the free energy.) Using the classical path approximation, Marko and Witten[14] used the RPA to study the stability of a blend of A–B end-grafted chains. They found that for sufficiently large incompatibility there could be instability in the lateral direction. The classical path approximation has also been combined with RPA to study the case of a grafting surface with negative curvature.[16]

We now consider the classical path approximation applied to the poor solvent situation. Since the classical path approximation is valid in the limit of $\gamma \to \infty$, it is inappropriate as a description of the small-γ and the crossover regimes. In the large-γ regime, $\langle c(z)\rangle$ in the classical path solution has a discontinuous jump at the layer height[17,18] (for a poor solvent). The jump in $\langle c(z)\rangle$ is equal to c_0, and $c(z) > c_0$ in the entire grafted layer. Therefore, within the classical path approximation, the RPA correction is stabilizing over the entire layer. This is also true of the step function profile.[15] On the other hand, our analysis shows that the mean field solution is unstable in the limit of $\gamma \to \infty$. The difference is that, at large γ, one expects (and we indeed find) that the linear instability affects a region smaller than $O(N)$ in the direction normal to the surface.[27] The classical path approximation loses the ability to describe structures on length scales smaller than $O(N)$ in this direction. Consequently, on this longer length scale, $O(N)$, the mean field profile is stable.[28]

VI. Summary

We have combined the random phase approximation with the numerical mean field analysis to study the case of an end-grafted homopolymer layer in a poor solvent. We found that as the solvent quality is decreased, the grafted layer is unstable to fluctuations tangential to the grafting plane. We constructed the phase diagram as a function of chain length, grafting density, and solvent quality, separating the regimes in which the laterally homogeneous layer is linearly stable from that in which it is linearly unstable. In a poor solvent and for fixed grafting density, we find that the grafted layer is always unstable to tangential fluctuations as the chain length is increased. For small values of the parameter $\gamma = N(w_3^2a^4)/(|w_2|^2l^4)$, we find that in the tangential direction the instability occurs at length scales on the order of X_0, the radius of gyration of the chain in a Θ-solvent. In the normal direction, the instability occurs over essentially the entire grafted layer. As γ is increased, the instability becomes restricted to the tip of the layer on a length scale on the order of the bulk correlation length. In the lateral direction, the instability occurs at length scales larger than X_0.

To summarize, our linear stability analysis indicates that in a poor solvent the grafted layer forms a dimpled surface in which both the depth of and the distance between the dimples depend on chain length, solvent quality, and grafting density. Our method does not require an analytic mean field solution and is therefore quite general. This approach should allow one to study the effect of fluctuations in a large class of spatially inhomogeneous polymer systems.

Acknowledgment. We are grateful to P. Y. Lai for fruitful discussions, we thank K. L. Huang, W.-X. Li, and T. A. Issaevitch for useful comments, and we thank M. Fasolka, who helped with some of the figures. A.C.B. is grateful to the Office of Naval Research through Grant N00014-91-J-1363 and the Department of Energy through Grant DE-FG02-90ER45438. D.J. thanks the National Science Foundation for support under Grant DMR89-14621.

Appendix A

In this appendix, we derive the rescaling used to obtain our two dimensionless parameters γ and β. This is the same rescaling as that used by Zhulina et al.[18] We can rewrite the many-chain Edwards Hamiltonian (eq 2.1) as

$$\mathcal{H}\{\mathbf{R}_b(m)\} = \sum_b \int_0^N dm \frac{1}{2a^2}\left|\frac{\partial \mathbf{R}_b(m)}{\partial m}\right|^2 + \frac{w_2 a^3}{2} c(\mathbf{R}_b(m)) + \frac{w_3 a^6}{3} c(\mathbf{R}_b(m))^2 \quad \text{(A1)}$$

with the condition

$$\frac{1}{A}\int d\mathbf{x}\int dz\, c(\mathbf{r}) = \int dz\, c(z) = N/l^2$$

Here A is the total area of the grafting surface and $c(z)$ is the concentration averaged over the x–y directions.

We now introduce the dimensionless variables appropriate for a poor solvent, $\tilde{z} = z/h$, $s = m/N$, $\tilde{\mathbf{x}} = \mathbf{x}/X_0$, and $\tilde{c} = c/c_0$, where $X_0^2 = a^2N/2$ and $c_0 = |w_2|/(w_3a^3)$. In terms of these dimensionless variables, the Hamiltonian becomes

$$\mathcal{H}\{\tilde{\mathbf{R}}_b(s)\} = \sum_b \frac{1}{4}\int_0^1 ds \left|\frac{\partial \tilde{\mathbf{X}}_b}{\partial s}\right|^2 + \frac{h^2}{4X_0^2}\int_0^1 ds \left|\frac{\partial \tilde{Z}_b}{\partial s}\right|^2 - \frac{h^2}{2X_0^2}\frac{2X_0^2Nw_2^2}{h^2w_3}\int_0^1 ds \left(\frac{1}{2}\tilde{c}(\tilde{\mathbf{R}}_b) - \frac{1}{3}\tilde{c}(\tilde{\mathbf{R}}_b)^2\right) \quad \text{(A2)}$$

and

$$\int d\tilde{z}\, \tilde{c}(\tilde{z}) = \frac{Nw_3a^3}{|w_2|hl^2}$$

where we have assumed that $w_2 < 0$. Letting $h = Nw_3a^3/(|w_2|l^2)$, $\gamma = h^2/(2X_0^2) = N(w_3^2a^4)/(|w_2|^2l^4)$, and $\beta = 2NX_0^2w_2^2/(h^2w_3) = (w_2^4l^4)/(w_3^3a^4)$, we obtain

$$\mathcal{H}\{\tilde{\mathbf{R}}_b(s)\} = \sum_b \gamma\int_0^1 ds \left(\frac{1}{2}\left|\frac{\partial \tilde{Z}_b}{\partial s}\right|^2 - \beta\left(\frac{1}{2}\tilde{c}(\tilde{\mathbf{R}}_b) - \frac{1}{3}\tilde{c}(\tilde{\mathbf{R}}_b)^2\right)\right) + \sum_b \frac{1}{4}\int_0^1 ds \left|\frac{\partial \tilde{\mathbf{X}}_b}{\partial s}\right|^2 \quad \text{(A3)}$$

and

$$\int d\tilde{z}\, c(\tilde{z}) = 1$$

Therefore the model is described by only two dimensionless parameters γ and β. Note that h results from straightforward dimensional analysis for the layer height in the strong stretching limit. Since $\gamma = h^2/X_0^2$, γ describes how much the chain is stretched in the z direction relative to its lateral extension. The variable β is more difficult to interpret physically. We can think of it as a measure of the strength of the interaction term versus the connectivity terms.

We may rewrite the two-body terms using

$$\sum_b \frac{1}{2}\int_0^N dm\, c(\mathbf{R}_b(m)) = \frac{1}{2}\int d\mathbf{r}\, c(\mathbf{r})^2 \qquad \text{(A4)}$$

$$= \int d\mathbf{r}\, c(\mathbf{r})\, \langle c(\mathbf{r})\rangle - \frac{1}{2}\int d\mathbf{r}\, \langle c(\mathbf{r})\rangle^2 + \frac{1}{2}\int d\mathbf{r}\, (\delta c(\mathbf{r}))^2$$

$$= \sum_b \int_0^N dm\, \langle c(\mathbf{R}_b)\rangle - \frac{1}{2}\int d\mathbf{r}\, \langle c(\mathbf{r})\rangle^2 + \frac{1}{2}\int d\mathbf{r}\, (\delta c(\mathbf{r}))^2$$

A similar expression may be obtained for the three-body term. Treating $\langle c(\mathbf{r})\rangle$ as an external field and dropping all terms in the Hamiltonian without explicit dependence on the chain trajectories, $\mathbf{R}_b(m)$, and terms of order δc^2 or higher, we obtain the mean field Hamiltonian $\mathcal{H}_0$ (eq 2.3). If we furthermore assume that the mean field solution is laterally homogeneous, $\mathcal{H}_0$ can be written in terms of the rescaled variables as $\mathcal{H}_0 = \gamma\tilde{\mathcal{H}}_0$, where $\tilde{\mathcal{H}}_0$ is given by

$$\tilde{\mathcal{H}}_0\{\tilde{Z}_b(s)\} = \sum_b \int_0^1 ds \left[\frac{1}{2}\left|\frac{\partial \tilde{Z}_b}{\partial s}\right|^2 - \beta(\langle \tilde{c}(\tilde{Z}_b)\rangle - \langle \tilde{c}(\tilde{Z}_b)\rangle^2)\right] \qquad \text{(A5)}$$

We have dropped all the $\mathbf{X}$ dependence, which can be integrated out in the partition function. The mean field partition function $\mathcal{Z}$ becomes

$$\mathcal{Z} = \int \mathcal{D}\{\tilde{Z}\} \exp(-\gamma\tilde{\mathcal{H}}_0) \qquad \text{(A6)}$$

where the integration is over all chain trajectories. We see immediately that in the limit of γ large, one can ignore all trajectories except those that minimize the Hamiltonian $\tilde{\mathcal{H}}_0$. (To be more precise, one only needs to include all trajectories that have energies within $O(\gamma^{-1})$ of the energy-minimizing trajectories.) This is known as the classical path approximation.[10,11]

Appendix B

For completeness, we summarize the standard formulas for the average concentration $\langle c(z)\rangle$ and the mean field correlation matrix A^0 in terms of the Green's functions.

The average concentration is given by eq 2.2

$$\langle c(\mathbf{r})\rangle = \sum_b \int dm\, \langle \delta(\mathbf{r} - \mathbf{R}_b(m))\rangle \qquad \text{(B1)}$$

In terms of the Green's function this becomes

$$\langle c(\mathbf{r})\rangle = \sum_b \frac{\int d\mathbf{r}_E\, G(\mathbf{r}_E,N;\mathbf{r},m)\, G(\mathbf{r},N;\mathbf{X}_b,0)}{\int d\mathbf{r}_E\, G(\mathbf{r}_E,N;\mathbf{X}_b,0)} \qquad \text{(B2)}$$

where X_b is the grafting point of the bth polymer on the $z = 0$ plane.

Assuming that the mean field solution is laterally homogeneous, we can replace the sum over chains, Σ_b, by an integral over the grafting surface $l^{-2}\int d\mathbf{X}$. Using eq 3.3 for $G(\mathbf{r},m;\mathbf{r}',m')$, we find

$$\langle c(z)\rangle = \frac{1}{\mathcal{Z}l^2}\int dz_E \int_0^N dm\, F(z_E,N;z,m)\, F(z,m;0,0) \qquad \text{(B3)}$$

where the normalization constant $\mathcal{Z}$ is

$$\mathcal{Z} = \int dz_E\, F(z_E,N;0,0) \qquad \text{(B4)}$$

and we have used the fact that $\int d\mathbf{x}\, G_0(\mathbf{x},m;\mathbf{x}',m') = 1$.

The general correlation matrix is given by

$$A(\mathbf{r},\mathbf{r}') = \langle c(\mathbf{r})\, c(\mathbf{r}')\rangle - \langle c(\mathbf{r})\rangle\, \langle c(\mathbf{r}')\rangle = \sum_{a,b} \langle c_a(\mathbf{r})\, c_b(\mathbf{r}')\rangle - \langle c_a(\mathbf{r})\rangle\, \langle c_b(\mathbf{r}')\rangle \qquad \text{(B5)}$$

where $c_b(\mathbf{r})$ is the concentration due to the bth chain at point $\mathbf{r}$. In the mean field approximation the chains are independent so that all terms with $a \neq b$ cancel and A^0 is given by

$$A^0(\mathbf{r},\mathbf{r}') = \sum_a \langle c_a(\mathbf{r})\, c_a(\mathbf{r}')\rangle^0 - \sum_a \langle c_a(\mathbf{r})\rangle\, \langle c_a(\mathbf{r}')\rangle \qquad \text{(B6)}$$

With the assumption that $X_0^2 > l^2$, we can replace the sum over grafting points by an integral over the grafting surface,

$$A^0(\mathbf{r},\mathbf{r}') = l^{-2}\int d\mathbf{X}_0\, \langle c_1(\mathbf{r},\mathbf{X}_0)\, c_1(\mathbf{r}',\mathbf{X}_0)\rangle^0 - \langle c_1(\mathbf{r},\mathbf{X}_0)\rangle^0\, \langle c_1(\mathbf{r}',\mathbf{X}_0)\rangle^0 \qquad \text{(B7)}$$

Here, $c_1(\mathbf{r},\mathbf{X}_0)$ is the concentration at $\mathbf{r}$ due to a chain grafted at $\mathbf{X}_0$. In terms of the Green's functions this becomes[14]

$$A^0(\mathbf{r},\mathbf{r}') = \frac{1}{\mathcal{Z}l^2}\int dz_E \int_0^N dm \int_0^m dm'\, G_0(\mathbf{x},m;\mathbf{x}',m') \times [F(z_E,N;z,m)\, F(z,m;z',m')\, F(z',m';0,0) + F(z_E,N;z',m)\, F(z',m;z,m')\, F(z,m';0,0)] - \frac{1}{\mathcal{Z}^2 l^2}\int dz_E \int_0^N dm \int dz'_E \int_0^N dm' \times G_0(\mathbf{x},m+m';\mathbf{x}_0',0)\, F(z_E,m;0,0)\, F(z_E',m';0,0) \qquad \text{(B8)}$$

We then Fourier transform with respect to the $\mathbf{x}$ to obtain $A^0(z,z';q)$ (eq 3.6),

$$A^0(z,z';q) = \frac{1}{\mathcal{Z}l^2}\int dz_E \int_0^N dm \int_0^m dm'\, e^{-q^2(m-m')/2} \times [F(z_E,N;z,m)\, F(z,m;z',m')\, F(z',m';0,0) + F(z_E,N;z',m)\, F(z',m;z,m')\, F(z,m';0,0)] - \frac{1}{\mathcal{Z}^2 l^2}\int dz_E \int_0^N dm \int dz'_E \int_0^N dm'\, e^{-q^2(m+m')/2} \times F(z_E,m;0,0)\, F(z_E',m';0,0) \qquad \text{(B9)}$$

We use the above formula to calculate the independent chain correlation matrix. In our case we discretized space with $\Delta z = 1/2$ and set the maximum value of z sufficiently large that it did not affect the result. We then invert the resulting square matrix numerically to obtain $[A^0]^{-1}(z,z';q)$.

References and Notes

(1) Halperin, A.; Tirrell, M.; Lodge, T. P. In *Advances in Polymer Science*; Springer-Verlag: Berlin, 1991; Vol. 100, p 31.
(2) Milner, S. T. *Science* **1991**, *51*, 251.
(3) Doi, M.; Edwards, S. F. *The Theory of Polymer Dynamics*; Oxford University Press: London, 1986.
(4) Dolan, A. K.; Edwards, S. F. *Proc. R. Soc. London, Ser. A* **1975**, *343*, 427. Dolan, A. K.; Edwards, S. F. *Proc. R. Soc. London, Ser. A* **1974**, *337*, 509.
(5) Helfand, E.; Wasserman, Z. R. *Macromolecules* **1978**, *11*, 960.
(6) Scheutjens, J. M. H. M.; Fleer, G. J. *J. Chem. Phys.* **1979**, *83*, 1619. Scheutjens, J. M. H. M.; Fleer, G. J. *J. Chem. Phys.* **1980**, *84*, 178.
(7) Hong, K. M.; Noolandi, J. *Macromolecules* **1981**, *14*, 727. Hong, K. M.; Noolandi, J. *Macromolecules* **1983**, *16*, 1083.
(8) Shull, K. R. *Macromolecules* **1990**, *23*, 4769. Shull, K. R. *J. Chem. Phys.* **1991**, *94*, 5737.
(9) Helfand, E.; Tagami, Y. *Polym. Lett.* **1971**, *9*, 741. Helfand, E.; Tagami, Y. *J. Chem. Phys.* **1972**, *56*, 3587.
(10) Milner, S. T.; Witten, T. A.; Cates, M. E. *Europhys. Lett.* **1988**, *5*, 413. Milner, S. T.; Witten, T. A.; Cates, M. E. *Macromolecules* **1988**, *21*, 2610.

(11) Zhulina, E. B.; Borisov, O. V.; Pryamitsyn, V. A.; Birshtein, T. M. *Vysokomol. Soedin.* **1989**, *A31*, 185.
(12) De Gennes, P.-G. *Scaling Concepts in Polymer Physics*; Cornell University Press: Ithaca, NY, 1979.
(13) Leibler, L. *Macromolecules* **1980**, *13*, 1602.
(14) Marko, J. F.; Witten, T. A. *Phys. Rev. Lett.* **1991**, *66*, 1541. Marko, J. F.; Witten, T. A. *Macromolecules* **1992**, *25*, 296.
(15) Ross, R. S.; Pincus, P. *Europhys. Lett.* **1992**, *19*, 79.
(16) Ching, E. S.; Witten, T. A. *Europhys. Lett.* **1992**, *19*, 687.
(17) Shim, D. F. K.; Cates, M. E. *J. Phys. Fr.* **1989**, *50*, 3535.
(18) Zhulina, E. B.; Borisov, O. V.; Pryamitsyn, V. A.; Birshtein, T. M. *Macromolecules* **1991**, *24*, 140.
(19) Lai, P. Y.; Binder, K. *J. Chem. Phys.* **1992**, *96*, 586.
(20) Grest, G. S.; Murat, M. Exxon Research Preprint, 1992.
(21) Klushin, L. I., unpublished work.
(22) (a) In the Edwards Hamiltonian, it is imagined that a course graining has been carried out so that the "renormalized parameter" $w_2 = 0$ marks the separation between good and poor solvents. In other contexts, our procedure has been referred to as "renormalized mean field theory". (b) We can include the higher order terms in the interaction energy in other ways also, for example, using a Flory–Huggins form $\chi\phi(1-\phi) + (\phi \ln \phi)/N + (1-\phi)\ln(1-\phi)$. These higher order terms can also be generated using the mean field method of Hong and Noolandi.[7]
(23) See, for example: Chandrasekhar, S. *Hydromagnetic Stability*; Clarendon Press: Oxford, 1961.
(24) We assume $l^2 < X_0^2$ and replace the sum over grafts by an integral over the grafting surface. Due to this approximation, our analysis cannot describe the regime $l^2 \gg X_0^2$ in which the polymers behave as isolated chains.
(25) There are only two dimensionless parameters if the discrete numerical method describes the continuum model sufficiently well. We checked that our choices of Δm and Δz were sufficiently small to not have any major effect on our calculations.
(26) Birshtein, T. M.; Pryamitsyn, V. A. *Vysokomol. Soedin.* **1987**, *A29*, 1858.
(27) We note that structures smaller than $O(N)$ can be described either by including corrections to the classical path approximation or by use of extra energetics arguments in addition to the classical path approximation.
(28) Ross and Pincus[15] concluded that any instability, if it exists, must be restricted to length scales less than the layer height (in the strong stretching limit).